Structurally tuned lead magnesium titanate perovskite as a photoelectrode material for enhanced photoelectrochemical water splitting

Sundaram Chandrasekaran[a], *Eui Jung Kim*[a], *Jin Suk Chung*[a], *Velusamy Senthilkumar*[b], *Yong Soo Kim*[c], *Chris R Bowen*[d], *Vaia Adamaki*[d], *Seung Hyun Hur*[a*]

[a]School of Chemical Engineering, University of Ulsan, Daehak-ro, 102, Nam-gu, Ulsan 680-749, South Korea
Corresponding Author: shhur@ulsan.ac.kr

[b] Department of Applied Physics, Papua New Guinea University of Technology, Lae, PMB, Papua New Guinea.

[c] Department of Physics and Energy Harvest Storage Research Center (EHSRC), University of Ulsan, Ulsan, South Korea.

[d] Department of Mechanical Engineering, University of Bath, Bath, BA2, 7AY, U.K

Abstract

First time, four distinct types of Lead Magnesium Titanate (PMT) perovskites including spheres, flakes, hierarchical flower and thin microbelts shaped were finely tuned via facile solution method to develop cost effective and high performance photoanode material for water splitting. The influence of solvent effects during structural tuning, purity, morphology, optical obsorption, structural phase transition and stoichiometric formation of prepared Lead Magnesium Titanate perovskites has been discussed in detail. Remarkably, thin microbelts structured PMT perovskite (PMTT) exhibited an excellent water splitting performance and it is more sensitive to the illuminated visible light. Owing to the unique structural features, the photoconversion efficiency value of PMTT perovskite is ~3.9, 3.54, 2.85 and 1.52 times higher than those of other prepared PMT perovskites including pristine $PbTiO_3$. The excellent water splitting performance of PMTT (thin microbelts) may be ascribed to the remarkable structural features that include a large surface area, high optical absorbance, more active sites and high interface area of the microbelts, which provide large contact areas between the electrolyte and highly active materials for electrolyte diffusion and a rapid route for charge transfer with minimal diffusion resistance. In addition, each thin microbelt is directly in contact with the Ni foam substrate, which can also shorten the diffusion path for the electrons. The demonstrated approach paves the way to significantly low-cost and high-throughput production of next generation, high performance and highly active water splitting perovskite photocatalyst.

Keywords: Perovskites, $PbTiO_3$, Lead Magnesium Titanate, Water splitting, microbelt

1. Introduction

Since the late 19th century, perovskite materials have had a dominant position within the portfolio of compounds, offering promise for next generation, high performance and ultralow-cost renewable energy storage and optoelectronic devices due to their unique chemical and physical properties[1-4]. Developing perovskite based photocatalyst materials that can efficiently split water under visible light is a significant technical challenge[5]. Thus, the development of water-splitting photocatalysts with a more narrow bandgap and a larger wavelength range is the most significant target for efficient solar hydrogen production. In this aspect, a number of perovskites and compounds with a layered perovskite structure are of interest (e.g. $MgTiO_3$, $CaTiO_3$, and $SrTiO_3$) which have photocatalytic activities for water splitting under light irradiation[6, 7] and exhibit several advantages such as enhanced charge separation, excellent thermal stability, and high chemical stability etc., Recently, it has been reported that solution-processed perovskites reveals extended electronic carrier diffusion lengths, large optical absorption coefficients and remarkable photovoltaic device performance [8-10]. In general, ABO_3 perovskite-types of the ferroelectric group are common but it is difficult to tailor nanostructures because they readily form highly symmetric cubic structures (**Fig. 1**) during synthesis [11-15]. Among the various methodologies and applications, direct water splitting using a single spinel type perovskite photocatalyst is attractive due to its simplicity, and is likely to be the most cost-effective approach to achieve large-scale solar hydrogen production[5, 7, 16, 17], but it is also regarded as the most challenging because there are more strict requisites compared to other nanostructured systems. In addition, the structurally tuned lead and titanate based organic or inorganic perovskites hold great promise for energy storage device applications as they can offer a vast array of other interesting structural possibilities[18-26]. Furthermore, from a structural viewpoint, the thin microbelt structure attracts attention compare to other structures such a spheres, flakes, flowers and rods especially for energy storage material applications. Among the potential structures, thin

microbelts are an unusual geometrical shape, that exhibit a high charge transfer, high surface area and porosity, elevated work functions, etc. in contrast to the other 1D, 3D nano/micro structures, and has stimulated extensive research attention[27-30]. Previously, a superior electrochemical performance has been observed for porous Fe_3O_4/C micro belts, which showed a high rate of lower charge-transfer resistance, large surface area and volume expansion effect etc [31]. Jyh Ming Wu et al reported that $ZnSnO_3$ microbelts can acts as a self-powered piezotronic strain sensor and single nanobelt sensor [32] and a $ZnSnO_3$ microbelts based nanogenerator exhibited a high energy conversion efficiency [33] of 4.2-6.6%. Moreover, upon the addition of microbelts with nanofibers, the luminescencent property of the material was greatly enhanced for YVO4:Ln material[34]. Shouying Huang et al[35] reported that, owing to the unique and superior properties of macroporous carbon microbelts, the structures are the best sorbents for organic pollutions. Yu Zhao et al reported[28] that, highly oriented (001) face Bi_2S_3 microbelts having a high surface work function compared to other nano structures such as spheres, flakes, flowers and this types of microbelts structures and its high work function make it favorable for photoanode materials. Qunhong Weng et al[30] reported porous microbelts of boron nitride are the best materials for high performance hydrogen storage. Therefore, it is highly desirable to develop a simple strategy to effectively fabricate novel and highly complex nanostructure arrays for energy harvesting applications. In this regard, the formation of structurally tuned PMT perovskite nanostructures, including a nanospheres, flakes, hierarchical flowers and thin sized microbelts were fabricated on the conductive Ni foam via facile, cost-effective solution method as shown in **Scheme 1.** During synthesis these four distinct types of perovskite structures were finely tuned by solvent effects. To our knowledge, these types of lead magnesium titanate (PMT) structures and its impact in Photoelectrochemical cell (PEC) water splitting system has yet to be explored. For samples identification, the prepared PMT nanospheres, PMT flakes, PMT hierarchical flowers and PMT thin microbelt shaped perovskite samples are named as PMTS,

PMTF, PMTH and PMTT, respectively. The origin of structural formation and transformation mechanisms, physical-chemical configurations, and their impact in terms of PEC water splitting will be discussed in detail. Among the various structures prepared in this study, the thin microbelt shaped PMT show the most promising performance, which allows it to be used as a cost effective and highly active water splitting perovskite photocatalyst.

2. Experimental section

2.1 Synthesis of various shaped nano PMT perovskites

Prior to the experimental procedure, the Ni foam (density-320 g m^{-2}, pore size-680 μm, thickness-1.7 mm, Hittite Co., Ltd, S. Korea) substrates were cleaned by a standard procedure, 1 M HCl treatment followed by deionized (DI) water washing. Typically, the PMT perovskites were grown on the vertically positioned pre-cleaned Ni foam. In brief, to synthesize PMTS, equal amounts of (i.e. 0.01 mole) $Pb(NO_3)_2$, $MgCl_2.6H_2O$ and $Ti(OCH(CH_3)_2)_4$ were initially dissolved in the 30 ml of aqueous solution of water and methanol (1:1 ratio) while constantly stirring at 70 °C. Then, 1 ml of acetic acid solution was added after 10 min followed by constant stirring for 1 h. During the entire reaction, the beaker was covered with a Petri dish to allow the CO_2 from air to diffuse into the system. After 1 h, 15 ml of water and ethanol (1:1 ratio) mixture was added dropwise to the precursor. After 3 hrs, the sample was washed with DI water several times and was carefully placed in a 70 °C oven for 1 h. The same condition has been adopted for $PbTiO_3$ synthesis except the addition of $MgCl_2.6H_2O$. The PMTF, PMTH and PMTT was grown using the same procedure except that the ethanol was replaced by sodium hydroxide (NaOH), heptane (C_7H_{16}) and isopropyl alcohol (C_3H_7OH), respectively. The final products have the mass loading of ~ 2.59, 2.62, 2.63, 2.61 and 2.63 mg/cm^2 of $PbTiO_3$, PMTS, PMTF, PMTH and PMTT respectively on Nickel foam.

2.2 Instrumental analysis

Field emission scanning electron microscopy (FE-SEM) images, elemental mapping and energy dispersive spectra (EDS) were obtained using a JEOL JSM 6500F scanning electron microscope. Microstructures were characterized by high-resolution transmission electron microscopy (HR-TEM, JEM-ARM200F). The crystallographic structure and chemical composition of the samples were determined using powder X-ray diffraction (XRD, Rigaku-X-ray diffractometer with Cu Kα radiation). An Analytik Jena SPECORD210 Plus UV–Vis spectrometer was used to obtain the optical absorption spectra. The chemical compositions and oxidation states of the perovskites were analyzed using a Thermo Scientific K-alpha X-ray photoelectron spectroscopy (XPS) instrument. Finally, N_2 adsorption - desorption measurements were carried out at 77 K using a Micromeritics ASAP 2020 gas-sorption system.

2.3 Photoelectrochemical measurements

Photoelectrochemical tests were performed using an electrochemical workstation (IvimStat, IVIUM Tech) at room temperature. Electrochemical measurements of a three-electrode cell system were carried out. The system was composed of nanostructured perovskites on Ni foam (1 cm × 1 cm) as the working electrode, a platinum (Pt) wire as the counter electrode, and an Ag/AgCl as the reference electrode. The other side of the working electrode (i.e. back side of perovskites on Ni foam) was masked with epoxy resin. Freshly prepared 0.1 M aqueous Na_2SO_4 solution was used as the electrolyte. The PEC performance was determined by a solar simulator (10500, Abet Tech, Xe lamp, AM 1.5 global filter, one sun power). Finally, the measured potential vs Ag/AgCl were converted to the Reversible Hydrogen Electrode (RHE) scale using the Nernst equation[16]. All experiments executed with a sweep rate of 20 mV/ sec.

3. Results and Discussion

The particle size, morphology and composition of the prepared perovskite samples are determined using FE-SEM, HR-TEM and EDS tools. FE-SEM images of the initial pure Ni foam and pristine $PbTiO_3$ sample are shown in **Fig. S1.** The surface morphology of the prepared PMT perovskites are shown in **Fig. 2** and **Fig. 3**, while all these structures were synthesized almost at the same reaction temperature and only the reactant content in the reaction mixture was different. The **Table S1** reveals the summarized chemical composition of prepared PMT perovskites by EDAX analysis. It is essential to comment that the structures were well reproducible when the growth condition was kept unchanged. The microscopic images of PMTS perovskites sample is shown in **Fig. 2(a-e)** clearly indicates that the PMTS forms 40-50 nm sphere like nanocrystals that are uniformly dispersed with minor aggregation. The microscopic images of PMTS perovskite sample and their corresponding elemental mappings and EDS spectra (**Fig. S2**) are evidence that the initial growth condition has a significant influence on the formation of nano and/or micro structures and chemical composition of the final material. During sphere shaped PMT synthesis, the ethanol reactant can be dispersed in water more homogeneously, thus the nucleation growth is subjected to less confinement in a boiling droplet solvent [36-38], and therefore a sphere-like structure is preferred. When we vary the mixture solvent by NaOH during synthesis of PMT perovskites, the solvent effect exhibit flake like structures as shown in **Fig. 2(f-j),** and clearly shows that the PMTF perovskites exhibit highly compact and intertwined flakes clusters. The ordered micro/nano-sized flakes are uniformly distributed in parallel to each other. **Fig. S3** shows their corresponding elemental maps and EDS spectra. Compared to PMTS sample, the PMTF perovskite the nano-flakes lie along to the Ni foam and are interconnected with each other, making a more opened pore channel [39, 40]. From a growth point of view**,** when the PMT nucleates at the substrate, the crystallographic orientation of the substrate will influence the

orientation of the final product, resulting in epitaxial structures. Moreover, the additions of acetic acid also enhances the porosity and fine-tuning the structure of the final materials[41, 42]. The anisometric shape of the flakes is probably caused by anisotropic surface energy[43]. However, the size of the nanostructures (i.e nucleation rate and growth events) can be tuned to some extent by varying the mixture of solvents (NaOH). One of the most important properties of a solvent is its polarity and a more polar solvent has a greater ability to couple with the hydrothermal energy, leading to a rapid increase in temperature and fast reaction rate during synthesis. This facilitates easy diffusion and homogeneous nucleation of the reacting species while also allowing for the formation of crystalline stoichiometric materials at low temperatures. However, the replacement of the solvent mixture by heptane yields hierarchical flower shaped architecture of PMT arrays on Ni foam as shown in **Fig. 2(k-o)** for the PMTH sample and their corresponding elemental maps and EDS spectra are presented in **Fig. S4**. From the microscopic morphological view, it can be seen that a large amount of hierarchical flowers are formed on the surface of Ni foam. It is showed that, the hierarchical flower-shaped is not a simple aggregation of small crystallites, but it is also composed of nano flakes growing homocentrically[44-46] as shown in **Fig. 2(m-o)**. By Diffusion-Limited Aggregation (DLA) theory[47], the variable aggregation level could be associated with the ability of the different solvents to disperse the nanocrystals during synthesis.

The FE-SEM and HR-TEM images in **Fig. 3(a-h)** show the thin sized micro belt structure (nano thickness) of the PMT perovskite. It clearly shows that the belt shaped PMT perovskites are formed on the surface of the Ni foam, where a small amount of flowers like structure are also grown on the surface of the thin sized micro belts. In addition, the **Fig. 3(i)** and **Fig. 3(j-m)** show the chemical composition and elemental mapping of the PMTT sample. The employment of isopropanol as a solvent may decrease the supercritical point of reaction solution and accelerate the reaction rate during various micro and nano structure synthesis[48-50]. Mallikarjuna et al reported that, due to the solvent density, long length Au and Pt

nanowire with ~10 nm thickness were obtained using isopropanol solvent[51]. Besides, it is reported that the elongated direction of the nanorods and/or thin belts is in the (001) direction (polar direction) of the tetragonal perovskite structure[52]. The self-assembly growth into nano sized thin belts in the (001) direction is probably highly influenced by the dipole interaction between individual nanocrystals because of their ferroelectric polarizations[53, 54]. In addition, the use of acetic acid has been shown to be necessary for the formation of nano thin belts/rods [41, 55-58]. The thickness of a typical PMT microbelt is ~50-70 nm, as shown in **Fig. 3c**. From all these viewpoints of growth behavior, the formation of this morphology is mainly attributed to weak basicity afforded by isopropanol, acetic acid and the cation[59-62]. Additionally, the stability of the (110) faces of the thin microbelts hinders further growth in the radial direction and promotes growth in the (001) direction for thin microbelts[54, 63, 64], which is also confirmed by HR-TEM image as shown in **Fig. 3h**. The formation of the carbonaceous layer on such structures should be avoided, as it prevents the nucleation of PMT on the substrate surface. Optimization of both the synthesis method and the synthesis parameters may result in homogeneous growth of PMT nano flakes, hierarchical flowers and thin belts over the entire substrate.

The XRD patterns of pristine $PbTiO_3$ and PMT perovskites shown in **Fig. 4a** reveal that the prepared samples are crystallized into the perovskite phase without any secondary phase and possess good crystallinity. As summarized in **Table S2**, the pristine $PbTiO_3$ and the PMT have the tetragonal phase and the pseudo-cubic structure, respectively, and are in good agreement with those previously reported[65-67], which can be also further supported by the presence of well resolved (001)-(100) and (002)-(200) doublets peaks around 2θ of 22-24° and 44-46°, respectively, in the $PbTiO_3$ perovskites. The two peaks of each doublet overlap, which indicates the development of pseudo-cubic symmetry that can be available for a high Mg concentration[67]. This behavior is mainly ascribed to the difference in the ionic radius of the Pb^{2+}, Ti^{4+} and Mg^{2+} ions. The substitution of Pb and/or Ti ions by Mg, presenting smaller

ionic radius, induces shrinkage of the lattice by the direct consequence a decrease in the cation/anion (*c/a*) ratio. In addition to the structural change, the change of the *c/a* ratio induces a change in the incorporation process on the two main sites and a variation of the total amount and nature of structural vacancies created for the charge compensation induced by the substitution of the main ions by the dopants[68]. The changes in the lattice constants indicated that magnesium atoms have been systematically dissolved into the crystal structure.

The chemical compositions of the PMT samples have been further investigated using XPS spectra. The XPS survey spectrum of PMT perovskites (**Fig. S5**) shows the presence of only Pb, Mg, Ti and O in the samples, and the detailed peak positions and compositions are summarized in **Table S3** and **Table S4**. As shown in the **Fig. 4b**, the peaks of $Pb4f_{7/2}$ and $Pb4f_{5/2}$ in the PMTT perovskites are at 137.68 and 142.58 eV, respectively, and are separated by ~5.1±0.1eV, which is similar to those previously reported values[69]. The XPS core-level spectrum of Mg1s **(Fig. 4c)** shows that the core level binding energy of Mg1s is at ~1303.68 eV. As shown in **Fig. 4d, f**or the Ti2p core levels, the 2p3/2 (459.07 eV) and 2p1/2 (464.66 eV) doublet exhibits an energy gap of ~5.6 eV, which is comparable to that reported for $PbTiO_3$[69]. The core level O1s XPS spectrum is shown in **Fig. 4e**. All the perovskite samples exhibited peaks with the major peak at a lower binding energy of ~530.83-531.45 eV, which corresponds to the lattice oxygen of PMT. No other impurities were detected by XPS and EDAX analysis, which indicate the high purity of the perovskite samples fabricated in this study.

The UV-Vis absorption spectra of pristine $PbTiO_3$ and various PMT perovskites are shown in **Fig. S6**. The absorbance of the PMTT perovskite has increased, which may be due to the contribution of increased surface charges of the perovskites that can modify the fundamental process of the electron-hole pair formation[70-72]. The optical band gap values of $PbTiO_3$ (2.78 eV), PMTS (2.66), PMTF (2.58 eV), PMTH (2.47 eV) and PMTT (2.33 eV)

have been evaluated according to the UV-Vis absorbance spectra by the Tauc relation from the onset of the absorption edges as described in **Fig. S6**. Similar to previous results[70-72], the perovskites prepared in this study exhibit a narrower band gap after the modification of composition and nanostructuring of the PMT. In addition, the red shift in the absorption edge of the PMTT perovskites compared to that of pristine $PbTiO_3$ also indicates the doping effect and tailored structural effect, which is beneficial to the energy harvesting performance especially for the visible light sensitive performances.

Fig. 5(a-b) shows the PEC water splitting results using various perovskite photoelectrodes including bare Ni foam when subjected to linear sweeping under dark and light illumination. As shown in **Fig. 5b**, the thin belt shaped PMTT exhibits a photocurrent density of ~ 1.77 mA cm^{-2} at 1.23 V vs RHE under light illumination and it is about ~ 4.52 times that of the pristine PMT (0.39 mA cm^{-2} at 1.23 V vs RHE), which can be ascribed to the high optical absorbance of PMTT perovskite sample (**Fig. S6**). More importantly, the synthesis method also provides a route to tailor the relevant electronic functions as described above. The charge carrier mobility could be enhanced along the microbelts direction by optimizing the stacking and π-π* interactions (**Fig. S6**). Note that the photocurrent achieved in this study is among the highest achieved with PMT perovskite without further water oxidation catalytic treatment and is also comparable with previously reported PEC performances using various perovskite type electrodes (**Table S5**). Upon further increase in potential, the current density can increase to as high as 2.85 mA cm^{-2} at 1.50 V versus RHE. In addition, the PMTS, PMTF and PMTH samples showed a maximum photocurrent density values of 0.521, 0.513 and 1.18 mA cm^{-2} at 1.23 V vs RHE respectively, which are lower than that obtained from PMTT but higher than that obtained by the pristine PMT. It is shown that using the porous nickel foam as a skeleton, the prepared PMT structures have an outstanding electronic conductivity because the sphere, flake, hierachial flower and thin microbelt shaped PMT active materials are tightly attached to the nickel foam, achieving

excellent adhesion and electrical contact[73-75]. As a result of the sphere, flake, hierarchical and thin microbelt features of these perovskite there is an increase in the amount of electroactive sites and improvement of the electrolyte penetration, which builds up a rapid way for charge transfer. Importantly, the enhanced performance achieved by the PMTT may due to this type of microbelt structure having particular advantages of high aspect ratio, high interfacial area, and the shortest pathway for ion diffusion, compared with other nanostructures[28, 30-33, 35, 50]. Previously, Liu et al[27], specified that $ZnCo_2O_4$ nanostructure/nickel foam architectures exhibit high specific capacitance (1400 F g^{-1} at 1 A g^{-1}) and excellent long-term cyclic stability. Mondal et al[76], reported, due to unique structural property of $NiCo_2O_4$ nanobelts (300-500 nm), the battery performance are superior compared to $NiCo_2O_4$ nanoflakes. In comparison to all other PMT perovskites, the thin microbelts configuration of the porous PMT perovskites/nickel foam exhibits a large surface area 66.64 m^2/g (**Fig. S7**), largest optical absorbance **(Fig. S6)** and this type of microbelts holds loose textures[27] with open spaces between neighboring belts[32, 33], these factors greatly increase the contact areas between the electrolyte and the thin microbelts, which improves electron/ion transport, enhances the kinetics of redox reactions, and facilitates stress relaxation during the water splitting reaction[73, 77]. Also, each thin microbelt directly contacts the Ni foam substrate, which can also shorten the diffusion paths of the electrons.

To further evaluate the performance of perovskite photoelectrodes, the photo conversion efficiency for each sample was calculated by the following equation;

$$\eta = I(1.23\text{-}V)/J_{light} \quad (1)$$

Where, V is the applied bias vs. RHE, I is the photocurrent density at the measured bias, and J_{light} is the irradiance intensity of 100 mW cm^{-2}. At a similar applied bias, the optimal conversion efficiency of $PbTiO_3$, PMTS, PMTF, PMTH and PMTT perovskite samples are shown in **Fig. 6a**. Initially, compared to the other samples including pristine $PbTiO_3$ the optimized PMTT perovskites exhibits significantly enhanced photoconversion efficiency of

1.57% and it is about ~ 3.9, 3.54, 2.85 and 1.52 times higher than those of pristine $PbTiO_3$, PMTS, PMTF and PMTH perovskites, respectively, which is consistent with the results obtained by J−V measurements shown in **Fig. 5b**. The highly extended light absorption band of PMTT perovskite is believed to make more photo-induced holes that contribute to the oxidation current under illumination. Compared to the various PMT electrodes, the microbelts structured PMT photoelectrodes may have higher efficiency due to their larger surface area exposed to the solution with minimum diffusion resistance. Such an interaction enables fast electron transfer between PMTT perovskite and Ni foam. Furthermore, the microbelts structure of PMT can also provide more conducting channels to transfer electrons between substrate and the surface of electrode, thus allowing the "long-range" electron transfer, which could increase the charge separation and suppress the charge recombination, thereby leading to the superior performance of the PMT microbelts. As shown in **Fig. 6b**, the light induced ON/OFF state proves that such thin microbelt based PMT photoanode is more sensitive to the illuminated visible light, and is effective in the generation and separation of electron-hole pairs and the electron transport to the counter electrode for water splitting. The results obtained in this study clearly suggest that the main determining factors of the PEC performance of a photoelectrode includes excellent optical absorbance, fine band gap tuning, optimized chemical compositions, structural modifications and the high surface area for energetic electron transport during water splitting mechanism.

4. Conclusion

In conclusion, we have demonstrated a unique and facile scalable fabrication procedure of regular arrays of nanospheres, flakes, hierarchical flowers and thin microbelts of lead magnesium titanate (PMT) with precisely controlled periodicity and aspect ratio, and have used them as photoelectrodes for water splitting. Our results have shown that the structurally engineered thin microbelts shaped PMT electrodes can significantly enhance

photon-capturing capability omnidirectionally as well as photoelectrode surface area, leading to a high photocurrent density there by rapid charge transfer. The findings in this work offer the rational design strategies for nanostructured perovskites for high performance PEC water splitting. The significant development validated here suggests that the purpose-built nanostructured architectures of perovskites are highly promising photoelectrodes for efficient PEC water splitting and further nano structural engineering can lead to more enhanced performances in the future. This new structurally tuned perovskites will give an outlook of future research avenues that might bring perovskite technology to commercialization.

Acknowledgement

This research was supported by Basic Science Research Program through the National Research Foundation of Korea (NRF) funded by the The Ministry of Science, ICT and Future Planning (NRF-2016R1A2B2006311).

References

[1] W. Wang, M. O. Tadé and Z. Shao. Research progress of perovskite materials in photocatalysis-and photovoltaics-related energy conversion and environmental treatment. *Chem. Soc. Rev.*, 44(2015) 5371-5408.

[2] M. Pena and J. Fierro. Chemical structures and performance of perovskite oxides. *Chem. Rev.*, 101(2001) 1981-2018.

[3] G. Xing, N. Mathews, S. S. Lim, N. Yantara, X. Liu, D. Sabba, M. Grätzel, S. Mhaisalkar and T. C. Sum. Low-temperature solution-processed wavelength-tunable perovskites for lasing. *Nat. Mater.*, 13(2014) 476-480.

[4] O. Malinkiewicz, A. Yella, Y. H. Lee, G. M. Espallargas, M. Graetzel, M. K. Nazeeruddin and H. J. Bolink. Perovskite solar cells employing organic charge-transport layers. *Nat. Photon.*, 8(2014) 128-132.

[5] J. Suntivich, K. J. May, H. A. Gasteiger, J. B. Goodenough and Y. Shao-Horn. A perovskite oxide optimized for oxygen evolution catalysis from molecular orbital principles. *Science.*, 334(2011) 1383-1385.

[6] F. E. Osterloh. Inorganic materials as catalysts for photochemical splitting of water. *Chem. Mater.*, 20(2007) 35-54.

[7] A. Kudo and Y. Miseki. Heterogeneous photocatalyst materials for water splitting. *Chem. Soc. Rev.*, 38(2009) 253-278.

[8] W. Nie, H. Tsai, R. Asadpour, J.-C. Blancon, A. J. Neukirch, G. Gupta, J. J. Crochet, M. Chhowalla, S. Tretiak and M. A. Alam. High-efficiency solution-processed perovskite solar cells with millimeter-scale grains. *Science.*, 347(2015) 522-525.

[9] J. You, Z. Hong, Y. M. Yang, Q. Chen, M. Cai, T.-B. Song, C.-C. Chen, S. Lu, Y. Liu and H. Zhou. Low-temperature solution-processed perovskite solar cells with high efficiency and flexibility. *ACS Nano.*, 8(2014) 1674-1680.

[10] Z. Xiao, C. Bi, Y. Shao, Q. Dong, Q. Wang, Y. Yuan, C. Wang, Y. Gao and J. Huang. Efficient, high yield perovskite photovoltaic devices grown by interdiffusion of solution-processed precursor stacking layers. *Energy Environ. Sci.,*7(2014) 2619-2623.

[11] P. Li, S. Ouyang, G. Xi, T. Kako and J. Ye. Li, Peng, et al. "The effects of crystal structure and electronic structure on photocatalytic H_2 evolution and CO_2 reduction over two phases of perovskite-structured $NaNbO_3$. *J. Phys. Chem. C.*, 116(2012) 7621-7628.

[12] M.-W. Chu, I. Szafraniak, R. Scholz, C. Harnagea, D. Hesse, M. Alexe and U. Gösele. Impact of misfit dislocations on the polarization instability of epitaxial nanostructured ferroelectric perovskites. *Nat. Mater.*, 3(2004) 87-90.

[13] I. Vrejoiu, M. Alexe, D. Hesse and U. Gösele. Functional perovskites–from epitaxial films to nanostructured arrays. *Adv. Fun. Mater.*, 18(2008) 3892-3906.

[14] R. L. Brutchey, E. S. Yoo and D. E. Morse. Biocatalytic synthesis of a nanostructured and crystalline bimetallic perovskite-like barium oxofluorotitanate at low temperature. *J. Am. Chem. Soc.*, 128(2006) 10288-10294.

[15] J. H. Kim, Y. M. Park and H. Kim. Nano-structured cathodes based on $La_{0.6}Sr_{0.4}$ $Co_{0.2}$ $Fe_{0.8}$ $O_{3-\delta}$ for solid oxide fuel cells. *J. Power Sources.*, 196(2011) 3544-3547.

[16] M. G. Walter, E. L. Warren, J. R. McKone, S. W. Boettcher, Q. Mi, E. A. Santori and N. S. Lewis. Solar water splitting cells. *Chem. Rev.*, 110(2010) 6446-6473.

[17] D. Ruzmetov, Y. Seo, L. J. Belenky, D. M. Kim, X. Ke, H. Sun, V. Chandrasekhar, C. B. Eom, M. S. Rzchowski and X. Pan. Epitaxial magnetic perovskite nanostructures. *Adv. Mater.*, 17(2005) 2869-2872.

[18] Y. Miseki, H. Kato and A. Kudo. Water splitting into H_2 and O_2 over niobate and titanate photocatalysts with (111) plane-type layered perovskite structure. *Energy Environ. Sci.*, 2(2009) 306-314.

[19] J. J. Choi, X. Yang, Z. M. Norman, S. J. Billinge and J. S. Owen. Structure of methylammonium lead iodide within mesoporous titanium dioxide: active material in high-performance perovskite solar cells. *Nano Lett.*, 14(2013) 127-133.

[20] P. Gao, M. Grätzel and M. K. Nazeeruddin. Organohalide lead perovskites for photovoltaic applications. *Energy Environ. Sci.*, 7(2014) 2448-2463.

[21] H. Liu, C. Hu and Z. L. Wang. Composite-hydroxide-mediated approach for the synthesis of nanostructures of complex functional-oxides. *Nano Lett.*, 6(2006) 1535-1540.

[22] Y. Mao, S. Banerjee and S. S. Wong. Large-scale synthesis of single-crystalline perovskite nanostructures. *J. Am. Chem. Soc.*, 125(2003) 15718-15719.

[23] H. Zheng, Q. Zhan, F. Zavaliche, M. Sherburne, F. Straub, M. P. Cruz, L.-Q. Chen, U. Dahmen and R. Ramesh. Controlling self-assembled perovskite-spinel nanostructures. *Nano Lett.*, 6(2006) 1401-1407.

[24] H. Zheng, J. Wang, S. Lofland, Z. Ma, L. Mohaddes-Ardabili, T. Zhao, L. Salamanca-Riba, S. Shinde, S. Ogale and F. Bai. Multiferroic $BaTiO_3$-$CoFe_2O_4$ nanostructures. *Science.*, 303(2004) 661-663.

[25] X. Zhu, Z. Liu and N. Ming. Perovskite oxide nanotubes: synthesis, structural characterization, properties and applications. *J. Mater. Chem.*, 20(2010) 4015-4030.

[26] P. M. Rørvik, T. Grande and M. A. Einarsrud. One-Dimensional Nanostructures of Ferroelectric Perovskites. *Adv. Mater.*, 23(2011) 4007-4034.

[27] B. Liu, B. Liu, Q. Wang, X. Wang, Q. Xiang, D. Chen and G. Shen. New energy storage option: Toward $ZnCo_2O_4$ nanorods/nickel foam architectures for high-performance supercapacitors. *ACS Appl. Mater. Interfaces.*, 5(2013) 10011-10017.

[28] Y. Zhao, X. Zhu, Y. Huang, S. Wang, J. Yang and Y. Xie, Synthesis, growth mechanism, and work function at highly oriented {001} surfaces of bismuth sulfide microbelts. *J. Phys. Chem. C.*, 111(2007) 12145-12148.

[29] Z.-G. Chen, C. Zhang, Y. Zou, E. Zhang, L. Yang, M. Hong, F. Xiu and J. Zou. Scalable Growth of High Mobility Dirac Semimetal Cd_3As_2 Microbelts. *Nano Lett.*, 15(2015) 5830-5834.

[30] Q. Weng, X. Wang, C. Zhi, Y. Bando and D. Golberg. Boron nitride porous microbelts for hydrogen storage. *ACS Nano.*, 7(2013) 1558-1565.

[31] L. Lang and Z. Xu. In situ synthesis of porous Fe_3O_4/C microbelts and their enhanced electrochemical performance for lithium-ion batteries. *ACS Appl. Mater. Interfaces.*, 5(2013) 1698-1703.

[32] J. M. Wu, K.-H. Chen, Y. Zhang and Z. L. Wang. A self-powered piezotronic strain sensor based on single $ZnSnO_3$ microbelts. *RSC Adv.*, 3(2013) 25184-25189.

[33] J. M. Wu, C. Xu, Y. Zhang and Z. L. Wang. Lead-free nanogenerator made from single ZnSnO3 microbelt. *ACS Nano.*, 6(2012) 4335-4340.

[34] Z. Hou, P. Yang, C. Li, L. Wang, H. Lian, Z. Quan and J. Lin. Preparation and luminescence properties of YVO_4: Ln and Y (V, P) O4: Ln (Ln= Eu^{3+}, Sm^{3+}, Dy^{3+}) nanofibers and microbelts by sol−gel/electrospinning process. *Chem. Mater.*, 20 (2008) 6686-6696.

[35] S. Huang and J. Shi. Monolithic macroporous carbon materials as high-performance and ultralow-cost sorbents for efficiently solving organic pollution. *Ind. Eng. Chem. Res.*, 53(2014) 4888-4893.

[36] L. Liang, X. Kang, Y. Sang and H. Liu. One-Dimensional Ferroelectric nanostructures: Synthesis, Properties, and Applications. *Adv. Sci.,* 1500358(2016) 1-21.

[37] S. Chandrasekaran. Synthesis of ZnO Nano Particles via Simple Solution Route for DSSC's Using Synthetic and Natural Dyes. *J. Nanoeng. Nanomanuf.* 1(2011) 242-247.

[38] S. Chandrasekaran, J. S. Chung, E. J. Kim and S. H. Hur. Exploring complex structural evolution of graphene oxide/ZnO triangles and its impact on photoelectrochemical water splitting. *Chem. Eng. J.*, 290(2016) 465-476.

[39] J. Du, G. Zhou, H. Zhang, C. Cheng, J. Ma, W. Wei, L. Chen and T. Wang. Ultrathin porous NiCo2O4 nanosheet arrays on flexible carbon fabric for high-performance supercapacitors. *ACS Appl. Mater. Interface.*, 5(2013) 7405-7409.

[40] X. Xiong, D. Ding, D. Chen, G. Waller, Y. Bu, Z. Wang and M. Liu. Three-dimensional ultrathin $Ni(OH)_2$ nanosheets grown on nickel foam for high-performance supercapacitors. *Nano Energy.*, 11(2015) 154-161.

[41] B. Xia, I. Lenggoro and K. Okuyama. Synthesis of CeO2 nanoparticles by salt-assisted ultrasonic aerosol decomposition. *J. Mater. Chem.*, 11(2001) 2925-2927.

[42] J.-Y. Gong, S.-H. Yu, H.-S. Qian, L.-B. Luo and X.-M. Liu. Acetic acid-assisted solution process for growth of complex copper sulfide microtubes constructed by hexagonal nanoflakes. *Chem. Mater.*, 18(2006) 2012-2015.

[43] M.-A. Einarsrud and T. Grande. 1D oxide nanostructures from chemical solutions. *Chem. Soc. Rev.*, 43(2014) 2187-2199.

[44] S. Chandrasekaran, S. H. Hur, W. M. Choi, J. S. Chung and E. J. Kim. Gold artichokes for enhanced photocatalysis. *Mater. Lett.*, 160(2015) 92-95.

[45] U. M. Patil, M. S. Nam, J. S. Sohn, S. B. Kulkarni, R. Shin, S. Kang, S. Lee, J. H. Kim and S. C. Jun. Controlled electrochemical growth of Co (OH) 2 flakes on 3D multilayered graphene foam for high performance supercapacitors. *J.Mater. Chem. A.*, 2(2014) 19075-19083.

[46] J. Cheng, Y. Lu, K. Qiu, H. Yan, X. Hou, J. Xu, L. Han, X. Liu, J.-K. Kim and Y. Luo. Mesoporous $ZnCo_2O_4$ nanoflakes grown on nickel foam as electrodes for high performance supercapacitors. *Phy.Chem. Chem. Phy.*, 17(2015) 17016-17022.

[47] J. Zhang, L. Sun, J. Yin, H. Su, C. Liao and C. Yan. Control of ZnO morphology via a simple solution route. *Chem. Mater.*, 14(2002) 4172-4177.

[48] C.-H. Lu, S.-Y. Lo and Y.-L. Wang. Glycothermal preparation of potassium niobate ceramic particles under supercritical conditions. *Mater. Lett.*, 55(2002) 121-125.

[49] J. Zhu, G. Zeng, F. Nie, X. Xu, S. Chen, Q. Han and X. Wang. Decorating graphene oxide with CuO nanoparticles in a water–isopropanol system. *Nanoscale.*, 2(2010) 988-994.

[50] H. G. Yang and H. C. Zeng. Creation of Intestine-like Interior Space for Metal-Oxide Nanostructures with a Quasi-Reverse Emulsion. *Angew. Chem. Int. Ed.,* 43(2004) 5206-5209.

[51] M. N. Nadagouda and R. S. Varma. Green and controlled synthesis of gold and platinum nanomaterials using vitamin B2: density-assisted self-assembly of nanospheres, wires and rods. *Green Chemistry.*, 8(2006) 516-518.

[52] B. O. Alawode and A. M. Kolpak. $PbTiO_3$ (001) Capped with ZnO ($11\bar{2}0$): An ab Initio Study of Effect of Substrate Polarization on Interface Composition and CO2 Dissociation. *J. Phys. Chem. Lett.*, 7(2016) 1310-1314.

[53] Z. Zhao, V. Buscaglia, M. Viviani, M. T. Buscaglia, L. Mitoseriu, A. Testino, M. Nygren, M. Johnsson and P. Nanni. Grain-size effects on the ferroelectric behavior of dense nanocrystalline $BaTiO_3$ ceramics.*Phys. Rev. B.*, 70(2004) 024107-024111.

[54] P. M. Rørvik, T. Grande and M.-A. Einarsrud. Hierarchical PbTiO3 nanostructures grown on SrTiO3 substrates. *Cryst. Growth Des.,* 9(2009) 1979-1984.

[55] G. Ren, M. N. F. Hoque, X. Pan, J. Warzywoda and Z. Fan. Vertically aligned VO 2 (B) nanobelt forest and its three-dimensional structure on oriented graphene for energy storage. *J.Mater. Chem. A.*, 3(2015) 10787-10794.

[56] Y. Yu, P. Li, X. Wang, W. Gao, Z. Shen, Y. Zhu, S. Yang, W. Song and K. Ding. Vanadium nanobelts coated nickel foam 3D bifunctional electrode with excellent catalytic activity and stability for water electrolysis. *Nanoscale.*, 8(2016) 10731-10738.

[57] H.-L. Zhang, F. Li, C. Liu and H.-M. Cheng. The facile synthesis of nickel silicide nanobelts and nanosheets and their application in electrochemical energy storage. *Nanotechnology.*, 19(2008) 165606-165612.

[58] J. M. Chin, E. Y. Chen, A. G. Menon, H. Y. Tan, A. T. S. Hor, M. K. Schreyer and J. Xu. Tuning the aspect ratio of NH2-MIL-53 (Al) microneedles and nanorods via coordination modulation. *CrystEngComm.*, 15(2013) 654-657.

[59] A. Weidenkaff. Preparation and application of nanostructured perovskite phases. *Adv.Eng. Mater.*, 6(2004) 709-714.

[60] T.-C. Tseng, C. Urban, Y. Wang, R. Otero, S. L. Tait, M. Alcamí, D. Écija, M. Trelka, J. M. Gallego and N. Lin. Charge-transfer-induced structural rearrangements at both sides of organic/metal interfaces. *Nat. Chem.*, 2(2010) 374-379.

[61] M. S. Read, M. S. Islam, G. W. Watson, F. King and F. E. Hancock. Defect chemistry and surface properties of $LaCoO_3$. *J. Mater. Chem.*, 10(2000) 2298-2305.

[62] J. E. Spanier, A. M. Kolpak, J. J. Urban, I. Grinberg, L. Ouyang, W. S. Yun, A. M. Rappe and H. Park. Ferroelectric phase transition in individual single-crystalline BaTiO3 nanowires. *Nano Lett.*, 6(2006) 735-739.

[63] K. Yasui and K. Kato. Dipole–dipole interaction model for oriented attachment of BaTiO3 nanocrystals: a route to mesocrystal formation. *J.Phys.Chem. C.*, 116(2011) 319-324.

[64] T. Yang, Z. D. Gordon and C. K. Chan. Synthesis of hyperbranched perovskite nanostructures. *Cryst. Growth Des.,* 13(2013) 3901-3907.

[65] L. S. Qiang, D. Y. Tang, X. H. Zhang and L. Jin, Solid State Phenomena, Trans Tech Publ: 2007; pp 149-152.

[66] F. Fadil, T. Lamcharfi, F. Abdi and M. Aillerie. Synthesis and characterization of magnesium doped lead titanate. *Cryst. Res. Technol.,* 46(2011) 368-372.

[67] J.-J. Shyu and K.-L. Mo. Characterization of sol-gel derived Mg-doped $PbTiO_3$ thin films. *J. Mater. Sci. Lett.,* 15(1996) 298-300.

[68] S. Gong, M. Li, Z. Ren, X. Yang, X. Li, G. Shen and G. Han. Polarization-Modified Upconversion Luminescence in Er-Doped Single-Crystal Perovskite $PbTiO_3$ Nanofibers. *J. Phys. Chem. C.*, 119(2015) 17326-17333.

[69] D. P. Dutta, B. P. Mandal, E. Abdelhamid, R. Naik and A. K. Tyagi. Enhanced magneto-dielectric coupling in multiferroic Fe and Gd codoped PbTiO 3 nanorods synthesized via microwave assisted technique. *Dalton Trans.*, 44(2015) 11388-11398.

[70] Y. Liu, W. Zhou, Y. Liang, W. Cui and P. Wu. Tailoring Band Structure of TiO_2 To Enhance Photoelectrochemical Activity by Codoping S and Mg. *J. Phys. Chem. C.*, 119(2015) 11557-11562.

[71] J. Singh, P. Kumar, K. S. Hui, K. Hui, K. Ramam, R. Tiwari and O. Srivastava. Synthesis, band-gap tuning, structural and optical investigations of Mg doped ZnO nanowires. *CrystEngComm.*, 14(2012) 5898-5904.

[72] S. Jiang, Z. Ren, S. Yin, S. Gong, Y. Yu, X. Li, X. Wei, G. Xu, G. Shen and G. Han. Growth and Bending-Sensitive Photoluminescence of a Flexible $PbTiO_3$/ZnO Nanocomposite. *ACS Appl. Mater. Interface.,* 6(2014) 10935-10940.

[73] J. Luo, J.-H. Im, M. T. Mayer, M. Schreier, M. K. Nazeeruddin, N.-G. Park, S. D. Tilley, H. J. Fan and M. Grätzel. Water photolysis at 12.3% efficiency via perovskite photovoltaics and Earth-abundant catalysts. *Science.*, 345(2014) 1593-1596.

[74] C. Tang, N. Cheng, Z. Pu, W. Xing and X. Sun. NiSe nanowire film supported on nickel foam: an efficient and stable 3D bifunctional electrode for full water splitting. *Angew. Chem. Int. Ed.*, 54(2015) 9351-9355.

[75] W. Zhou, X.-J. Wu, X. Cao, X. Huang, C. Tan, J. Tian, H. Liu, J. Wang and H. Zhang. Ni_3S_2 nanorods/Ni foam composite electrode with low overpotential for electrocatalytic oxygen evolution. *Energy Environ. Sci.,* 6(2013) 2921-2924.

[76] A. K. Mondal, D. Su, S. Chen, X. Xie and G. Wang. Highly porous $NiCo_2O_4$ nanoflakes and nanobelts as anode materials for lithium-ion batteries with excellent rate capability. *ACS Appl. Mater. Interface.,* 6(2014) 14827-14835.

[77] Y. Qiu, S.-F. Leung, Q. Zhang, B. Hua, Q. Lin, Z. Wei, K.-H. Tsui, Y. Zhang, S. Yang and Z. Fan. Efficient photoelectrochemical water splitting with ultrathin films of hematite on three-dimensional nanophotonic structures. *Nano Lett.*, 14(2014) 2123-2129.

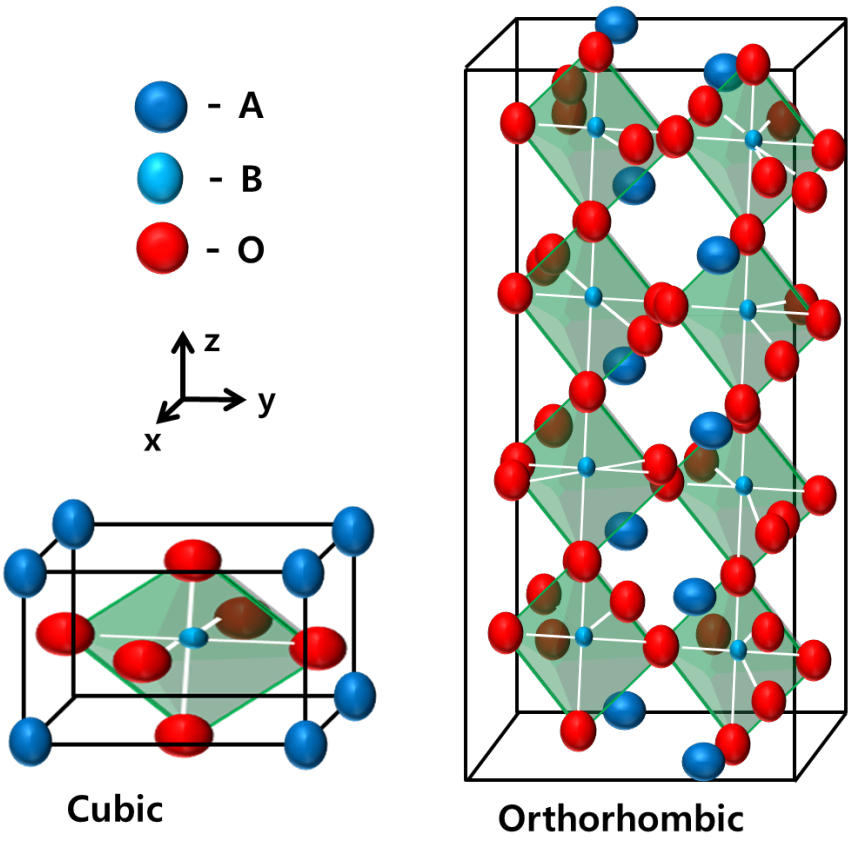

Fig. 1. Unit cell atomic arrangements of ABO_3 type perovskites and (b) its pseudo-cubic phase transformation

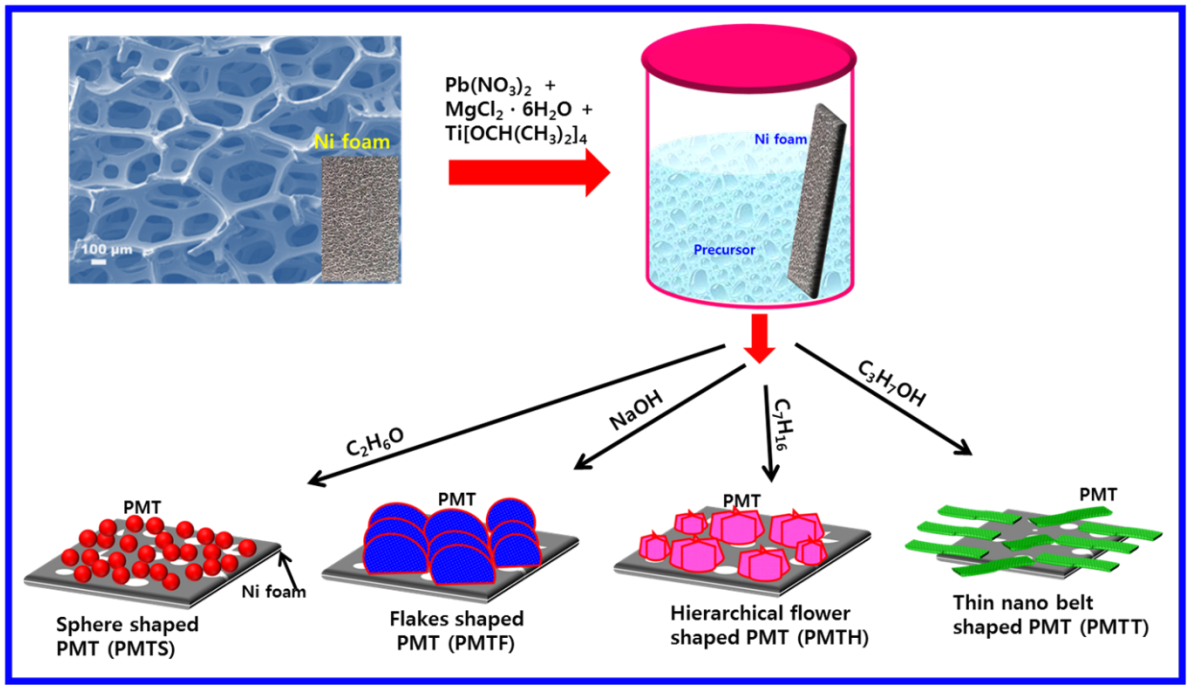

Scheme 1. Schematic diagram of synthesis of structurally tuned PMT perovskites

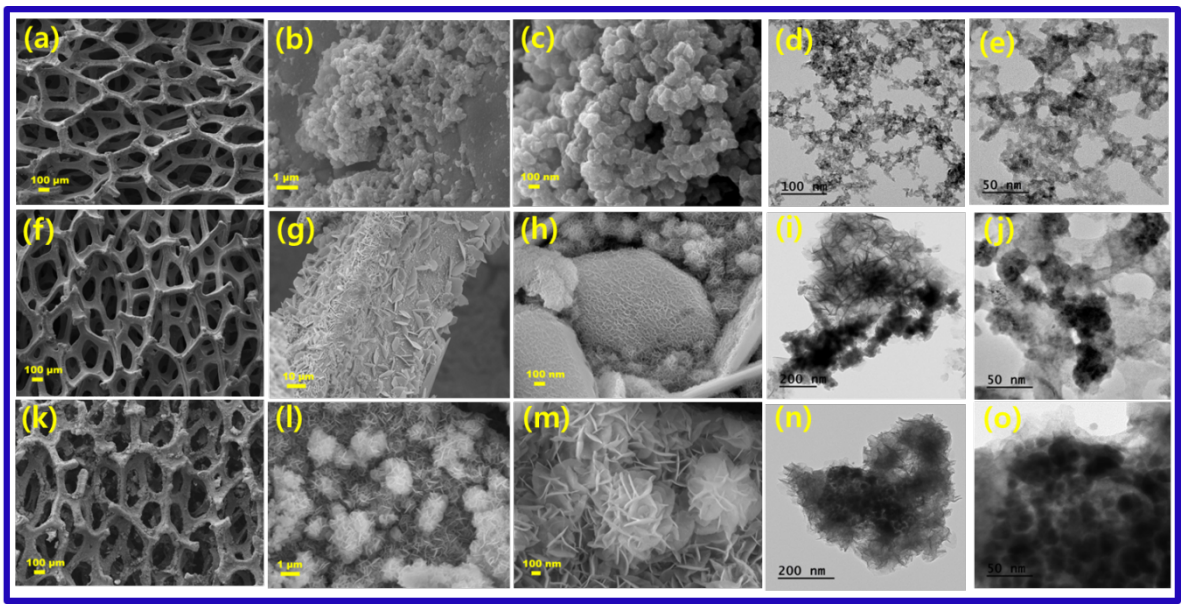

Fig. 2. (a-c); (f-h); (k-m) FE-SEM images and (d-e); (i-j); (n,o) HR-TEM images of PMTS (nanospheres), PMTF(nanoflakes) and PMTH (hierachial flowers) perovskites on the Ni foam respectively.

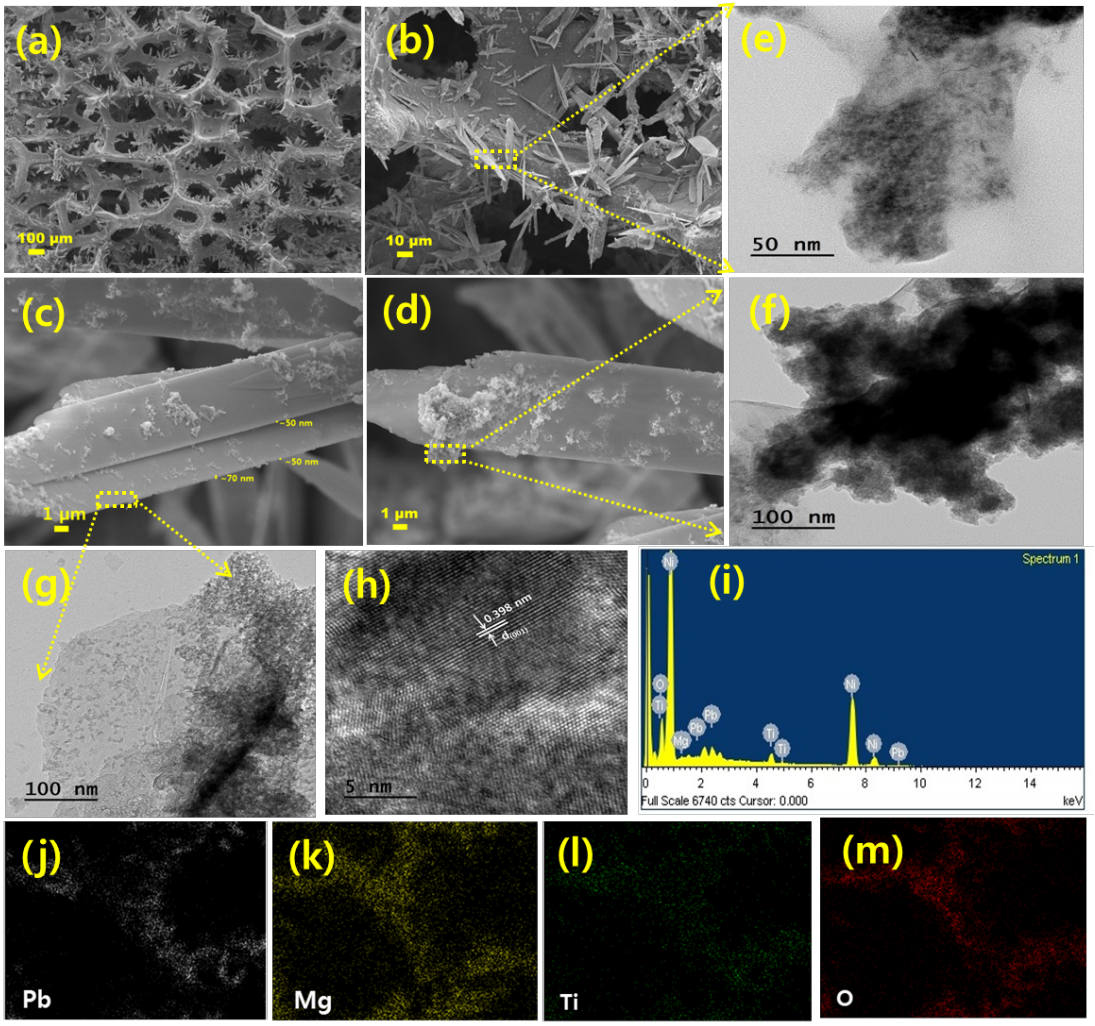

Fig. 3. (a-d) FE-SEM images and (e-h) HR-TEM images of PMTT perovskite sample. (i) EDAX spectra and (j-m) Elemental mapping diagram of Pb, Mg, Ti and O elements in PMTT perovskite sample.

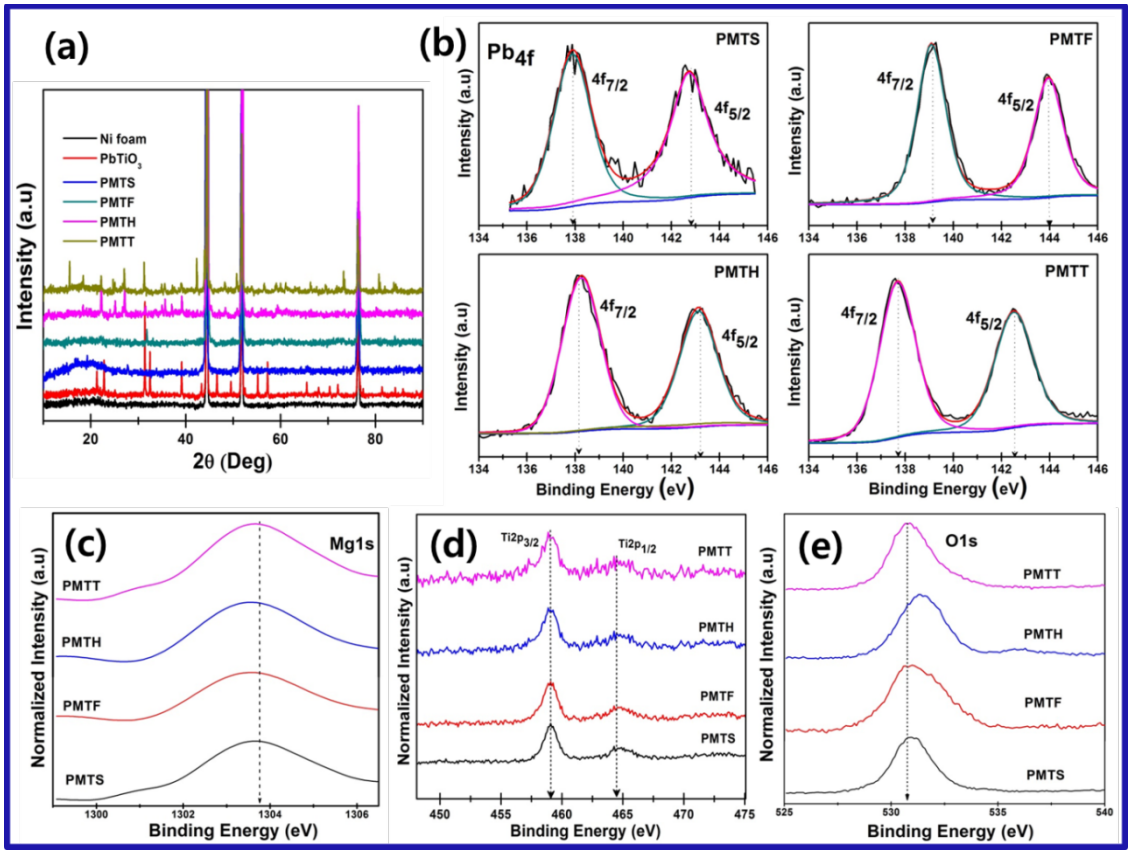

Fig. 4. (a) XRD patterns of pure Ni foam, pure $PbTiO_3$ and structurally tuned PMT perovskites. (b) XPS spectra of Pb4f, (c) Mg1s, (d) Ti2p and (e) O1s core-levels of structurally tuned PMT perovskites.

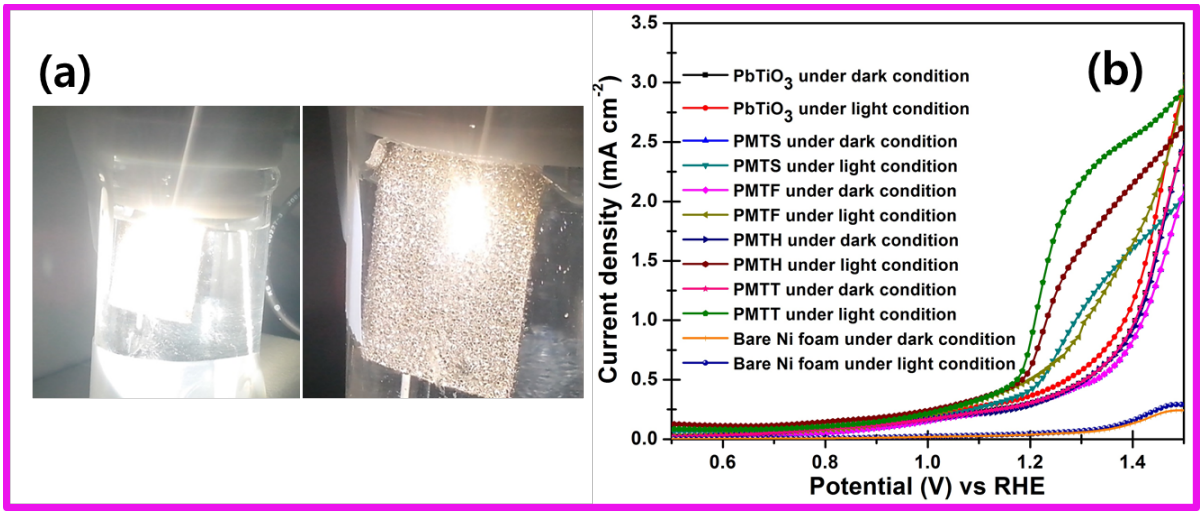

Fig. 5. (a) Digital photographic image of water splitting reaction in PMT photoelectrode (b) LSV curves of bare Ni foam and structurally tuned PMT photoelectrodes under dark and 1 sun power (100mW cm^{-2}) solar simulator with a scan rate of 20 mv/sec in 0.1 M Na_2SO_4. The mass loading of the samples were ~ 2.59, 2.62, 2.63 2.61 and 2.63 mg of $PbTiO_3$, PMTS, PMTF, PMTH and PMTT respectively on Nickel foam.

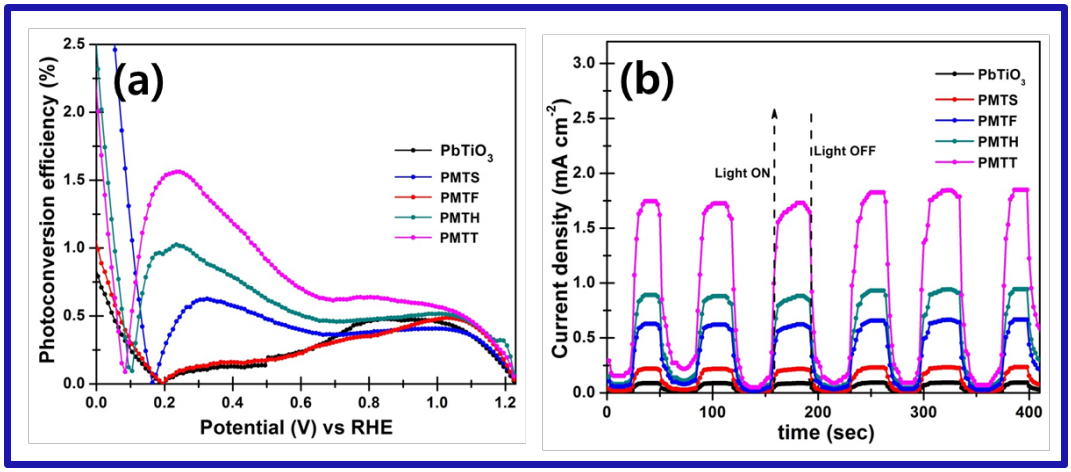

Fig. 6. (a) Photoconversion efficiency curves of structurally tuned PMT photoelectrodes under 1 sun power (100mW cm^{-2}) solar simulator with a scan rate of 20 mV/sec in 0.1 M Na_2SO_4 and (b) Time dependent photo-response in PMT photoelectrodes including pristine $PbTiO_3$ perovskite at fixed potential of 1.23 V Vs RHE. The mass loading of the samples were ~ 2.59, 2.62, 2.63, 2.61 and 2.63 mg of $PbTiO_3$, PMTS, PMTF, PMTH and PMTT respectively on Nickel foam.